33rd Annual International Conference of the IEEE EMBS
Boston, Massachusetts USA, August 30 - September 3, 2011

Atlas-based segmentation for globus pallidus internus targeting on low-resolution MRI

Maria I. Iacono, Nikos Makris, Luca Mainardi, John Gale, Andre van der Kouwe, Azma Mareyam, Jonathan R. Polimeni, Lawrence L. Wald, Bruce Fischl, Emad N. Eskandar, and Giorgio Bonmassar

Abstract—**In this paper we report a method to automatically segment the internal part of globus pallidus (GPi) on the pre-operative low-resolution magnetic resonance images (MRIs) of patients affected by Parkinson's disease. Herein we used an ultra-high resolution human brain dataset as electronic atlas of reference on which we segmented the GPi. First, we registered the ultra-high resolution dataset on the low-resolution dataset using a landmarks-based rigid registration. Then an affine and a non-rigid surface-based registration guided by the structures that surround the target was applied in order to propagate the labels of the GPi on the low-resolution un-segmented dataset and to accurately outline the target. The mapping of the atlas on the low-resolution MRI provided a highly accurate anatomical detail that can be useful for localizing the target.**

I. Introduction

PARKINSON's disease (PD) is the second most common neurodegenerative disease and more than 4 million people worldwide are affected. The early symptoms and signs of PD, namely rest tremor, bradykinesia and rigidity, are related to the progressive loss of nigrostriatal dopaminergic neurons [1].

Deep brain stimulation (DBS) of the internal part of the globus pallidus (GPi) has shown to significantly improve the motor symptoms of advanced PD patients who are no longer responsive to drug therapy. A process that significantly helps the neurosurgical DBS procedure is the accurate identification of GPi using a pre-operative magnetic resonance (MR) dataset. Currently, this is done by direct visualization, which is intrinsically limited because of the poor contrast and resolution of routine clinical images [2].

The recent introduction of 7 T MRI into clinical research has offered the possibility of investigating many anatomical details not detectable using weaker field scanners [2]. The enhanced visualization of small brain structures like basal ganglia nuclei can be used to achieve greater precision to guide DBS procedures to reach the desired targets.

Due to the unavailability of these powerful MRI scanners in the clinical practice, we have developed a method for exploiting the detailed information deriving from an ultra-high resolution human brain datasets in which the GPi is well defined. Herein we used this dataset as electronic atlas of reference on which the GPi was manually segmented. Subsequently, we used these data in an atlas-based segmentation procedure to outline the GPi on the pre-operative low resolution images of patients affected by PD. The mapping of the atlas on the pre-operative low-resolution MRI will provide a highly accurate anatomical detail that can be useful for the targets localization.

II. Materials and Methods

A. Experimental Protocol

A brain hemisphere was selected for the construction of the ultra-high resolution MRI-based atlas. A T2* MRI was acquired as follows: 100 μm^3 isotropic resolution, TR/TE/flip=40ms/20ms/20°, 1600×1100×896 matrix [3].

The 1 mm^3 resolution T1-weigthed MNI152 MRI provided by the Montreal Neurological Institute has been used as the low-resolution patient image to be segmented. This volume was spline-interpolated to create a high resolution volume with isotropic resolution of 100 μm^3.

B. Atlas-based Segmentation

The goal of the atlas-based segmentation is to find the transformation that registers the ultra-high resolution atlas, in which structures of interest have been labeled, to a new MRI dataset of a subject, in which those structures cannot be easily recognized, in order to propagate the labels on that dataset and to segment it according to the resulting transformation.

Since the volumes to be registered show significant differences (due to the different acquisition protocol, resolution, and informative content) the registration, in turn, need to be guided by a priori knowledge about the anatomy (i.e. by the segmentation) [4].

The global atlas-based segmentation procedure is composed by the following steps:

i. a manual segmentation of the GPi and structures useful for the surface-based registration;

ii. a preliminary landmark-based registration followed by a surface-based registration of the ultra-high resolution dataset (*floating*) on the MNI152 (*reference)*;

Manuscript received March 26, 2011.

M. I. Iacono is with A. A. Martinos Center for Biomedical Imaging, Dept. of Radiology, MGH, Charlestown, MA, USA. (phone: (+1) 617-726-0962; fax: (+1) 617-726-5711; e-mail: iacono@nmr.mgh.harvard.edu).

N. Makris, A. Van der Kouwe, A. Mareyam, J. Polimeni, L. Wald, B Fischl, and G. Bonmassar are with A. A. Martinos Center for Biomedical Imaging, Dept. of Radiology, MGH, Charlestown, MA, USA.

L. Mainardi is with the Biomedical Engineering Department, Politecnico di Milano, Italy.

J. Gale is with Cleveland Clinic, Department of Neuroscience and Center for Neurological Restoration, Cleveland, Ohio, USA.

E. Eskandar is with Neurosurgery, Massachusetts General Hospital, Boston, MA, United States

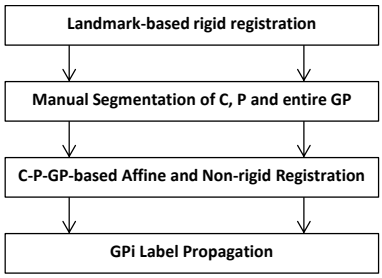

Fig.1. Atlas-based segmentation workflow.

iii. the GPi label propagation.

Fig. 1 shows the atlas-based segmentation workflow.

C. Manual Segmentation

The contours of the target nucleus (GPi) and the surrounding nuclei (caudate, putamen and the external part of the globus pallidus GPe) were manually outlined on the ultra-high resolution dataset (Fig. 2 *left*). The resulting output is a label mask, namely atlas. The atlas construction is performed only once and the same label mask can be used a number of times to segment new patients' MRIs.

The caudate (C) and the putamen (P) were manually segmented also on the patient dataset. Differently from ultra-high resolution dataset, the globus pallidus (GP) was segmented as a unique structure on patient data without discerning between its internal and external parts (Fig. 2 *right*).

The caudate, the putamen and the entire GP were chosen to guide registration since they enclose the target of interest and then they can incorporate in the registration process very localized information on the neighbourhood relationships. Furthermore, their contours can be easily recognized on typical routine MR images and then they can also be outlined on the low-resolution images using semi-automatic or automatic segmentation strategies [4].

Fig. 2 shows the 3D model of the basal ganglia and the axial, the sagittal and coronal views of the segmented structures on both the datasets.

D. Registration

The registration of the atlas on the MNI152 was performed by a preliminary landmark-based registration followed by a surface-based registration.

For the preliminary landmark-based affine registration a set of three non-collinear corresponding landmarks were manually identified in each volume: namely, the anterior commissure (AC), the posterior commissure (PC), and the superior point of the interhemispheric fissure.

The algorithm for direct computation of the transformation is straightforward involving alignment of the centroids of the two sets of points followed by rotation and scaling of the image to be registered to minimize the sum of the squared displacements between floating and reference points. Once the coarsest differences between the two volumes, due to the different orientation and position, were corrected, the ultra-high resolution atlas was further registered using a surface-based registration procedure.

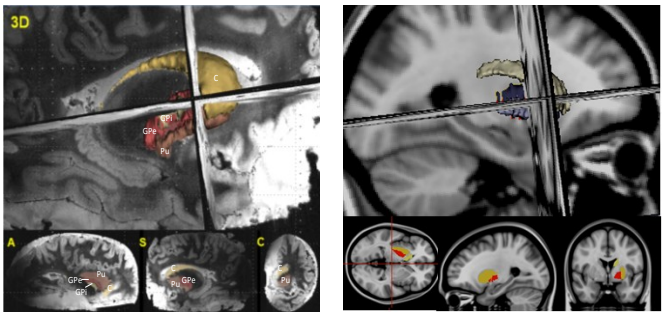

Fig.2. 3D model of the basal ganglia (top) and the axial (A), the sagittal (S), and coronal (C) views of the segmented structures (bottom) on the ultra-high resolution dataset (left) and on the MNI152 (right).

For the affine registration, different registration strategies were employed: each segmented structure (the caudate nucleus (C), the putamen (P) and the entire globus pallidus (GP)) or a combination of them (C-P, C-GP, P-GP, C-P-GP) in the atlas was registered with the corresponding one in the patient dataset using an affine registration based on the iterative closest point (ICP) algorithm [5].

ICP starts with two corresponding meshes, that were generated by directly triangulating the homologous structures [6], and uses as initial estimation for their relative transform the transformation resulting from the preliminary landmark-based registration. Then, it iteratively refines the transform by repeatedly generating pairs of corresponding points on the meshes and minimizing the sum of squared distances (SSD) between the points.

The algorithm stops when the difference between the SSD for successive iterations falls below 0.001 or a maximum number of 500 iterations is reached.

Finally, a non-linear version of ICP algorithm based on the entire set of the segmented nuclei was applied.

The non-linear registration was applied in a multi-resolution fashion by manipulating an underlying mesh of B-spline control points. The control points act as parameters of the free form deformations (FFDs) and the degree of deformation which can be modeled depends essentially on the resolution of the mesh of control points.

The accuracy of the transformation was measured by the root mean square error (RMSE).

E. GPi label propagation

Atlas-based segmentation methods view the segmentation problem as a registration problem: once the different transformations were estimated, they were used to deform the label masks from the atlas onto the patient image. The manual labels of the GPe and GPi which were manually outlined on the ultra-high resolution dataset, are therefore propagated on the MNI152 dataset (*label propagation*).

The lack of gold standards and the usual unavailability of a ground truth make the assessment of the label propagation accuracy difficult to solve. An estimate of the ground truth was obtained asking an anatomist to manually outline the GPi on the MNI152 on the basis of his anatomical knowledge. GPi is placed laterally with respect to the white matter of the internal capsule and medially to the external

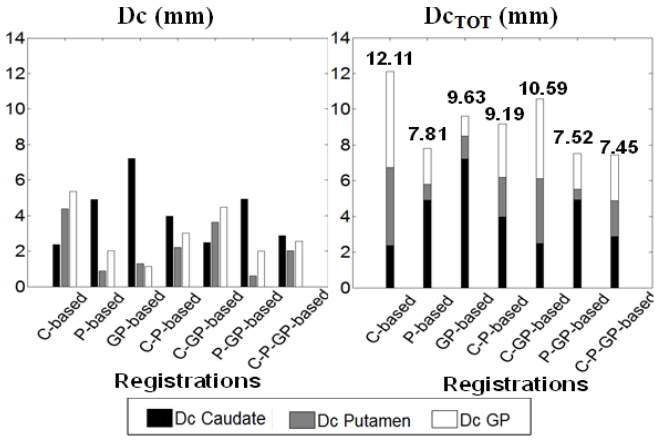

Fig.3. For each combination-based registration the distances between the centroids (Dc) of the algorithmically and the manually segmented structures (left) and the total Dc (right).

part of the globus pallidus (GPe). GPi and GPe are separated by white matter fibers, namely the medial medullary lamina.

Validation of GPi segmentation via label propagation was performed by evaluating several indices which compare the GPis semi-automatically identified by the registration procedures with that manually delineated by the anatomist.

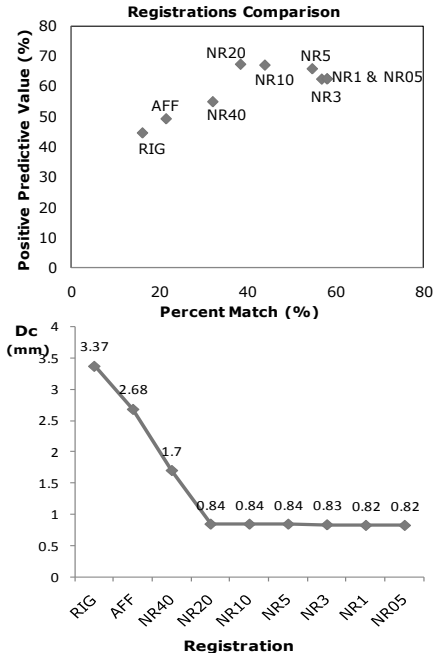

Fig.4. Comparison between different transformation models: PM and P+ (top) and Dc (bottom)

Distance between centroids

To benchmark the accuracy of the semi-automatic segmentation of GPi the distance between the centroids (Dc) of the semi-automatically and the manually outlined GPis was estimated.

Volumetric Overlap

Two different volumetric overlap metrics have been considered:

$$PM = \left[\frac{TP}{GT}\right]\cdot 100 = \left[\frac{TP}{TP+FN}\right]\cdot 100 \quad (1)$$

$$P+ = \left[\frac{TP}{TP+FP}\right]\cdot 100 \quad (2)$$

Where TP=true positives, i.e. pixels labeled as GPi in the GT and by the algorithm, FP=false positives, i.e. pixels labeled as GPi but not within GT, and FN=false negatives (FN), i.e. pixels falsely marked as background.

PM (Percent Match) index shows the correspondence between GT and algorithm segmentation. An ideal PM value is 100%, that means that the algorithm localizes perfectly GPi pixels. Conversely, the P+ (Positive Prediction Value) index estimates the correspondence in size and location between the algorithm segmentation and GT.

III. RESULTS

Fig. 3 shows for each structure-based (C-based, P-based, and G-based registration respectively) and combination-based registration (C-P-based, C-GP-based, P-GP-based, and C-P-GP-based registration) the distances between the centroids (Dc) of the algorithmically segmented and the manually segmented caudates (black bars), putamens (gray bars) and GPs (white bars) (left) and the total Dc that was calculated as the sum of the three distances (right).

P-based, C-P-based and P-GP registration show low values of Dc and this enables us to infer that the putamen has a significant influence on the structures location estimation through the registration process.

However, the better compromise was obtained when all three structures were used to guide the registration. We obtained for this last case a total Dc of 7.45 mm.

Fig. 4 summarizes the results of the segmentation quality in terms of PM versus P+ (top) and Dc (bottom) for the different transformation models when all the three structures were used to guide the registration. For each transformation model we plot PM and P+ index in a single graph. The best values will be located next to the right angle, in which PM and P+ index reach the ideal value of 100% (Fig. 4).

The results clearly show that affine registration (AFF) improves the quality of the segmentation as compared with rigid registration (RIG). However, both these transformation models perform significantly worse than the proposed non-rigid transformation model (NR). The results also show that

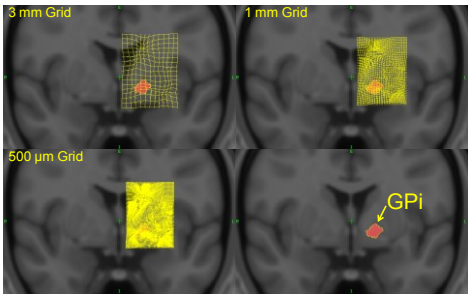

Fig.5. Deformation fields obtained using a 3 mm (top left), 1 mm (top right) and 500 µm (bottom left) control points resolution and the final segmentation of GPi (bottom right).

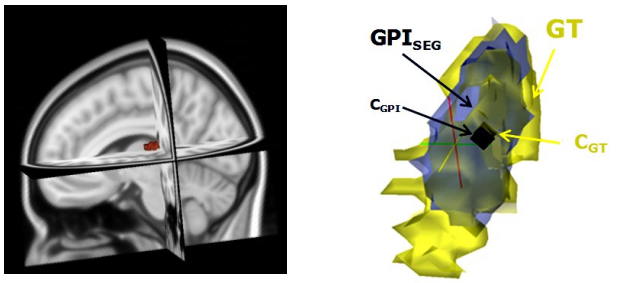

Fig.6. 3D reconstructed model of the algorithmically obtained GPi on the MNI152 (left) and its synchronous view with the ground truth (right)

the non-rigid registration performs better as the resolution of the control point mesh of the spline-based FFD increases. While a control point spacing of 40 mm (NR40) yields already high quality compared to affine transformations, a control point spacing of 10 (NR10) or 5 mm (NR5) yields even better results. The main reason for this is the increased flexibility of the spline-based FFD to describe local deformations as the number of control points increases. For grid spacing lower than 5 mm, if we further increase the resolution of the mesh the PM slightly increases (from 54.85 % to 57.01%) at the expense of P+ (from 65.68% to 62.29%), so a better match with respect to the anatomist manual outline is accompanied by a slight increase of false positives.

Regarding the accuracy of the transformation, we reach a RMSE of 492 μm, 450 μm and 432 μm for the 3 mm, 1 mm and 500 μm respectively.

In Fig. 5 the results of the non-linear registration are presented. The resulting deformed grids and the deformation fields are shown at the highest resolution levels. On the bottom right the final segmentation of the GPi on the MNI152 is shown.

Figure 6 shows the reconstructed 3D model of the GPi on the axial, the sagittal, and coronal views of the MNI152 (left) and the synchronous view of the semi-automatically segmented volume GPi_{SEG} and the GT volume (right).

As it seen, the algorithm underestimates the real volume of the GPi. This result is confirmed by the PM index that reaches a maximum value of 58.24% for the 500 μm resolution grid. However, the distance Dc between the GPi_{SEG} centroid (C_{GPI}) and the GT centroid (C_{GT}) results smaller (820 μm) than the dimension of the voxel on the low-resolution routine images (Fig. 6 right).

IV. CONCLUSIONS

In this paper, we proposed an ultra-high resolution atlas-based segmentation procedure to discriminate the GPi on the pre-operative low resolution images.

Validation issues are crucial especially in DBS procedures where targets are small and their localization difficult. Accurate preoperative targeting can reduce the need for invasive exploration and decrease procedure-related complications.

A study of surrounding visible easy-segmentable structures has revealed that the putamen is the nucleus that most influences the registration process. This is due to the strict topological relationship between putamen and GP that are nestled snugly together, giving the appearance of a lens shape with the convex surface oriented laterally.

The use of affine registration based on the simultaneous use of multiple nuclei followed by a further non-rigid registration demonstrated an improvement of the quality of the GPi segmentation. The quality further improved as the resolution of the control points mesh of the spline-based FFD increases. However, results neatly show that no significant performance improvement is achieved beyond a 3 mm grid resolution.

The GPi volume obtained using a final resolution grid of 500 μm results slightly underestimated compared with the manually outlined volume assumed as ground truth. However the estimate of its centroid, which is the most significant information for the planning of a trajectory in a targeted surgical procedure, is more accurate than the resolution commonly used for the routine MRI acquisitions.
The proposed approach was evaluated only on the MNI152. Therefore this limited data do not enable a robust quantitative assessment of the accuracy of the method.
However, this paper represents a first attempt to approach the problem and further investigations will be done. The method will be tested on a large number of cases in order to assess the generalizability of these findings to patients with different morphometry. Furthermore, in the absence of ground truth segmentation for clinical data, we adopted a golden standard generated by the anatomist using manual segmentation tools. It would be interesting to test the method using synthetic low resolution data for which a high-resolution segmentation is known.

Nevertheless our results on localizing the GPi were encouraging and we expect that the high resolution and the optimized contrast of the atlas may allow us to discriminate other DBS target structures such as the subthalamic nucleus (STN) in a way similar to the atlas-based segmentation procedure described for the GPi.

REFERENCES

[1] D. Twelves, K. S. Perkins, and C. Counsell, "Systematic review of incidence studies of Parkinson's disease," *Mov Disord*, vol. 18, pp. 19-31, 2003.

[2] Z.-H. Cho, H.-K. Min, S.-H. Oh, J.-Y. Han, C.-W. Park, J.-G. Chi, Y.-B. Kim, S. H. Paek, A. M. Lozano, and K. H. Lee, "Direct visualization of deep brain stimulation targets in Parkinson disease with the use of 7-tesla magnetic resonance imaging." *Journal of Neurosurgery*, vol. 113, pp. 639-647, 2010.

[3] M. Mareyam, J. Polimeni, J. Alagappan, B. Fischl, and L. Wald, " A 30 channel receive-only 7T array for ex vivo brain hemisphere imaging.," presented at 17th Scientific Meeting, International Society for Magnetic Resonance in Medicine, 2009.

[4] L. P. Clarke, R. P. Velthuizen, M. A. Camacho, J. J. Heine, M. Vaidyanathan, L. O. Hall, R. W. Thatcher, and M. L. Silbiger, "MRI segmentation: methods and applications," *Magn Reson Imaging*, vol. 13, pp. 343-68, 1995.

[5] P. Besl and N. MacKay, "A Method for Registration of 3-D Shapes," *IEEE Trans Pat Anal and Mach Intel*, vol. 14, pp. 239-56, 1992.

[6] W. E. Lorensen and H. E. Cline, "Marching cubes: A high resolution 3D surface construction algorithm." in *Proceedings of the 14th annual conference on Computer graphics and interactive techniques*: ACM, 1987, pp. 163-169.